Near-Field to Near/Far-Field Transformation for Arbitrary Near-Field Geometry, Utilizing an Equivalent Magnetic Current

Ardalan Taaghol and Tapan K. Sarkar

Abstract— **A method is presented for computing near- and far-field patterns of an antenna from its near-field measurements taken over an arbitrary geometry. This method utilizes near-field data to determine an equivalent magnetic current source over a fictitious surface which encompasses the antenna. This magnetic current, once determined, can be used to ascertain the near and the far fields. This method demonstrates that once the values of the electromagnetic field are known over an arbitrary geometry, its values for any other region can be obtained. An electric field integral equation is developed to relate the near fields to the equivalent magnetic current. A moment method procedure is employed to solve the integral equation by transforming it into a matrix equation. A least squares solution via singular value decomposition is used to solve the matrix equation. Computations with both synthetic and experimental data, where the near field of several antenna configurations are measured over various geometric surfaces, illustrate the accuracy of this method.**

I. Introduction

Presented here is a method for near-field to near/far field transformation which requires no specific geometry for near-field measurements. In this approach, by using the equivalence principle [1], an equivalent magnetic current replaces the radiating antenna. Furthermore, it is assumed that the near field is produced by the equivalent magnetic current and therefore, via Maxwell's equation from the measured near-field data, the current source can be determined. Once this is accomplished, the near field and the far field of the radiating antenna in all regions in space in front of the radiating antenna can be determined directly from the equivalent magnetic current.

An electric field integral equation is developed which pertains to the measured near fields and the equivalent magnetic current. This integral equation has been solved for the unknown magnetic current source through a moment method procedure [2] with point matching, where the equivalent current is expanded as linear combinations of two-dimensional (2-D) pulse basis functions and, therefore, the integral equation is then transformed into a matrix equation. In general, the matrix is rectangular whose dimensions depend on the number of field and source points chosen. The matrix equation is solved by the method of least squares via the singular value decomposition [3], [4]. By this, the moment matrix is decomposed into a set of orthogonal matrices which can be easily inverted.

Another aspect of this approach is that the numerical integrations in the process of creating the moment matrix elements have been avoided by taking a limiting case. Since the field points and the source points are to never coincide, and if their distances are much larger than the sizes of the current patches, then the pulse basis functions expanding the current source can be approximated by Hertzian dipoles [5].

The formulation and theoretical basis for the equivalent magnetic current approach along with the formation of the corresponding matrix equation using the method of moments and its solution using the method of least squares via singular value decomposition is presented in the following sections.

Manuscript received February 9, 1995; revised January 29, 1996. This work was supported in part by E. I. Dupont de Nemours and Company and by the CASE Center of Syracuse University.

The authors are with the Department of Electrical and Computer Engineering, Syracuse University, Syracuse, NY 13244 USA.

Publisher Item Identifier S 0018-9375(96)03860-4.

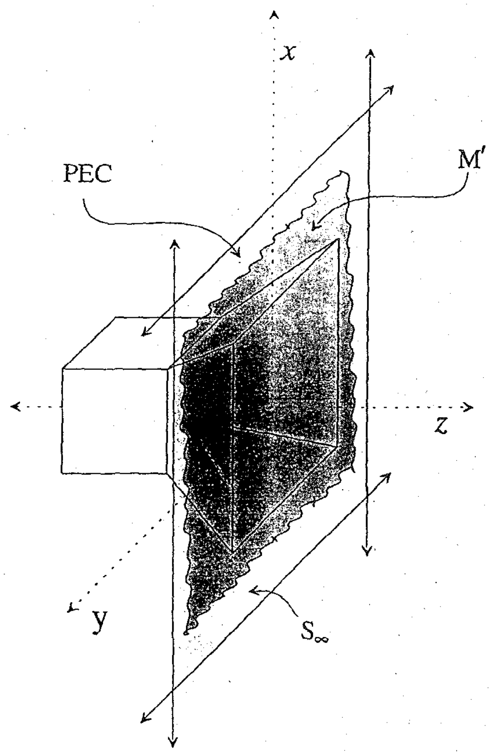

Fig. 1. Equivalent problem with a magnetic current sheet.

II. Formulation of the Electric Field Integral Equation by the Equivalent Magnetic Current Approach

Consider an arbitrarily shaped antenna radiating into free space. The aperture of the antenna is in a plane surface separating all space into left half and right half spaces as shown in Fig. 1. The aperture of the antenna is placed in the xy-plane and is facing the positive z-axis. Since we are interested only in the electromagnetic field in front of the radiating antenna (i.e., the space where $z > 0$), we place a perfect electric conductor, extending to infinity in the x- and y-directions, on the xy-plane in front of the aperture of the antenna (Fig. 1). By the equivalence principle [1], a surface magnetic current M' may be placed on this perfect electric conductor whose value is equal to the tangential value of the electric field on the xy-plane

$$M' = E \times \hat{n} \text{ on } S_\infty \tag{1}$$

where E is the electric field on the xy-plane, S_∞ is the entire xy-plane at $z = 0$, and $\hat{n}$ is the unit outward normal to the xy-plane pointing in the direction of the positive z-axis.

Using image theory [1], an equivalent magnetic current M can be introduced as

$$M = 2M' \tag{2}$$

radiating in free space. Therefore,

$$M = 2E \times \hat{n} \text{ on } S_\infty \tag{3}$$

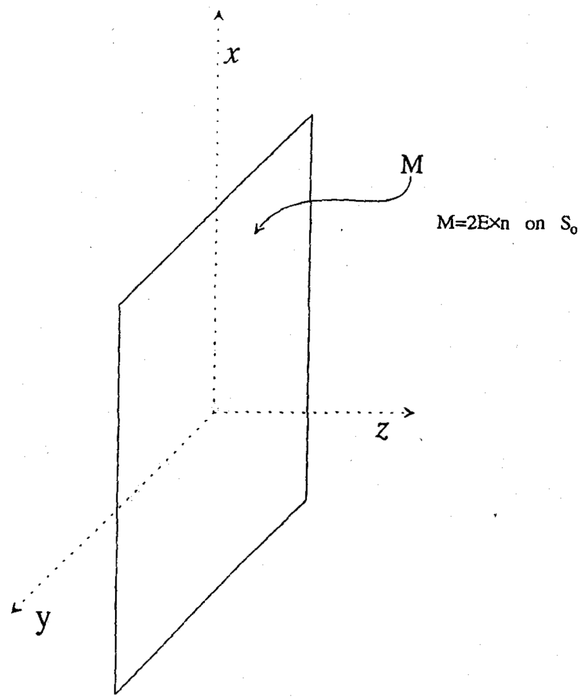

Fig. 2. Equivalent magnetic current covering the aperture of the antenna and radiating in free space.

where M now replaces the source antenna and radiates into free space (Fig. 2), producing exactly the same field as the original antenna in the region $z > 0$. The measured near field of the antenna may now be used to determine M from

$$E_{\text{meas}} = E(M) = -\frac{\nabla X}{4\pi}\int_{S_\infty} M(r')g(r;\, r')\,ds' \qquad (4)$$

where E_{meas} is the electric near field measured over a geometry at a distance away from the aperture of the radiating antenna. Here r is the field location and r' is the location of the source point and ∇ is the gradient operator in the cartesian coordinates. In addition, the free space Green's function $g(r;\, r')$ is given by

$$g(r,\, r') = \frac{e^{-jk_o|r-r'|}}{|r-r'|} \qquad (5)$$

and $k_o = 2\pi/\lambda$ where λ is the wavelength.

By assuming that the measured field points are far from the current carrying region S_o (S_∞ is the truncated to S_o for numerical computation as per Fig. 2), the equivalent magnetic current $\vec{M}$ can be expanded into Hertzian dipoles existing at the center of the 2-D patch as is conventionally done in the method of moments [5].

Therefore,

$$M_x(x',\, y') = \sum_{i=1}^{N_x}\sum_{j=1}^{N_y}\alpha_{ij}\,\Delta x\,\Delta y\,\delta(x'-x_i,\, y'-y_j) \qquad (6a)$$

$$M_y(x',\, y') = \sum_{i=1}^{N_x}\sum_{j=1}^{N_y}\beta_{ij}\,\Delta x\,\Delta y\,\delta(x'-x_i,\, y'-y_j) \qquad (6b)$$

where α_{ij} and β_{ij} are the unknowns be solved for. The effect of the δ-functions in (6) is to replace the integrals in (4) by their integrands evaluated at the positions of the δ-functions. Since the electric near field is known at discrete points on the geometry over which it has been measured, a point matching procedure [5] is chosen. Substituting (6) into (4) and utilizing point matching, the following matrix equation is obtained

$$\begin{bmatrix}\vec{E}_{\text{meas},\,\theta}\\ \vec{E}_{\text{meas},\,\phi}\end{bmatrix} = \begin{bmatrix}H_{11} & H_{12}\\ H_{21} & H_{22}\end{bmatrix}\begin{bmatrix}\vec{M}_x\\ \vec{M}_y\end{bmatrix} \qquad (7)$$

where $\vec{E}_{\text{meas},\,\theta}$ and $\vec{E}_{\text{meas},\,\phi}$ are column vectors whose elements are the θ- and ϕ-components of the electric near field, respectively, measured at discrete points. $\vec{M}_x$ and $\vec{M}_y$ are column vectors whose elements are the unknown coefficients α_{ij} and β_{ij}, respectively. H_{11}, H_{12}, H_{21}, and H_{22} are the submatrices of the entire moment matrix and are given by

$$[H_{11}]_{k,\,l} = \left\{\begin{array}{l}\cos\theta_k\sin\phi_k\frac{e^{-jk_0R_{k,\,l}}}{4\pi R_{k,\,l}^2}(z_k^f)\left[jk_0+\frac{1}{R_{k,\,l}}\right]\\ +\sin\theta_k\frac{e^{-jk_0R_{k,\,l}}}{4\pi R_{k,\,l}^2}(y_k^y-y_l^s)\left[jk_0+\frac{1}{R_{k,\,l}}\right]\end{array}\right\}\Delta x\,\Delta y \qquad (8a)$$

$$[H_{12}]_{k,\,l} = -\left\{\begin{array}{l}\cos\theta_k\cos\phi_k\frac{e^{-jk_0R_{k,\,l}}}{4\pi R_{k,\,l}^2}(z_k^f)\left[jk_0+\frac{1}{R_{k,\,l}}\right]\\ +\sin\theta_k\frac{e^{-jk_0R_{k,\,l}}}{4\pi R_{k,\,l}^2}(x_k^f-x_l^s)\left[jk_0+\frac{1}{R_{k,\,l}}\right]\end{array}\right\}\Delta x\,\Delta y \qquad (8b)$$

$$[H_{21}]_{k,\,l} = \left\{\cos\phi_k\frac{e^{-jk_0R_{k,\,l}}}{4\pi R_{k,\,l}^2}(z_k^f)\left[jk_0+\frac{1}{R_{k,\,l}}\right]\right\}\Delta x\,\Delta y \qquad (8c)$$

$$[H_{22}]_{k,\,l} = \left\{\sin\phi_k\frac{e^{-jk_0R_{k,\,l}}}{4\pi R_{k,\,l}^2}(z_k^f)\left[jk_0+\frac{1}{R_{k,\,l}}\right]\right\}\Delta x\,\Delta y \qquad (8d)$$

where θ_k and ϕ_k are the θ and ϕ coordinates, respectively, of the kth field measuring point and x_l^s, y_l^s are the x- and y-coordinates,

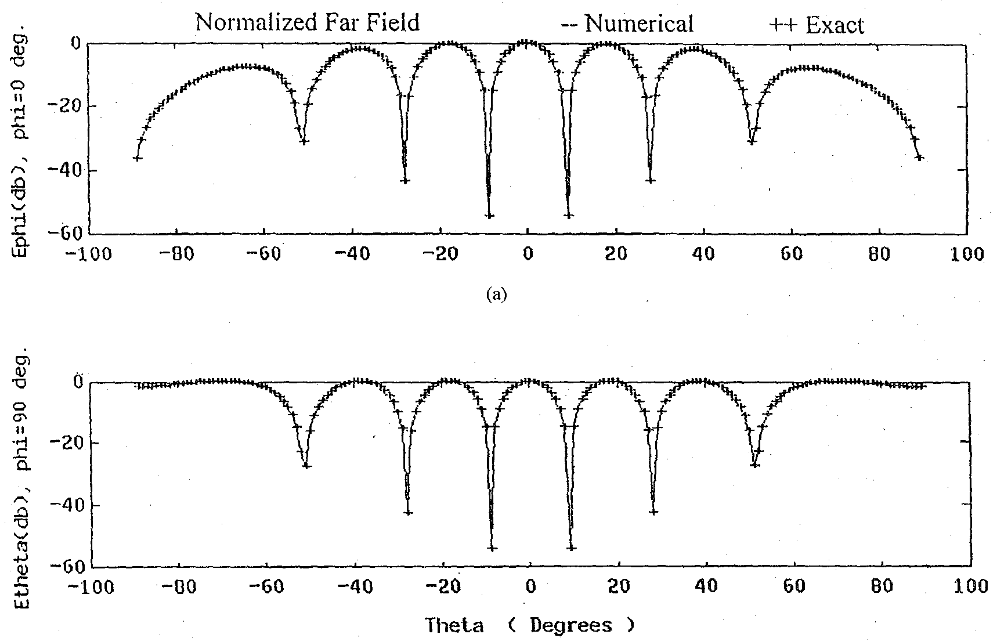

Fig. 3. (a) Comparison of exact and computed far field $\phi = 0°$ and $90°$ cut for a 2×2 electric dipole array on a $3.6\lambda \times 3.6\lambda$ surface. (b) Near field was measured on an arc.

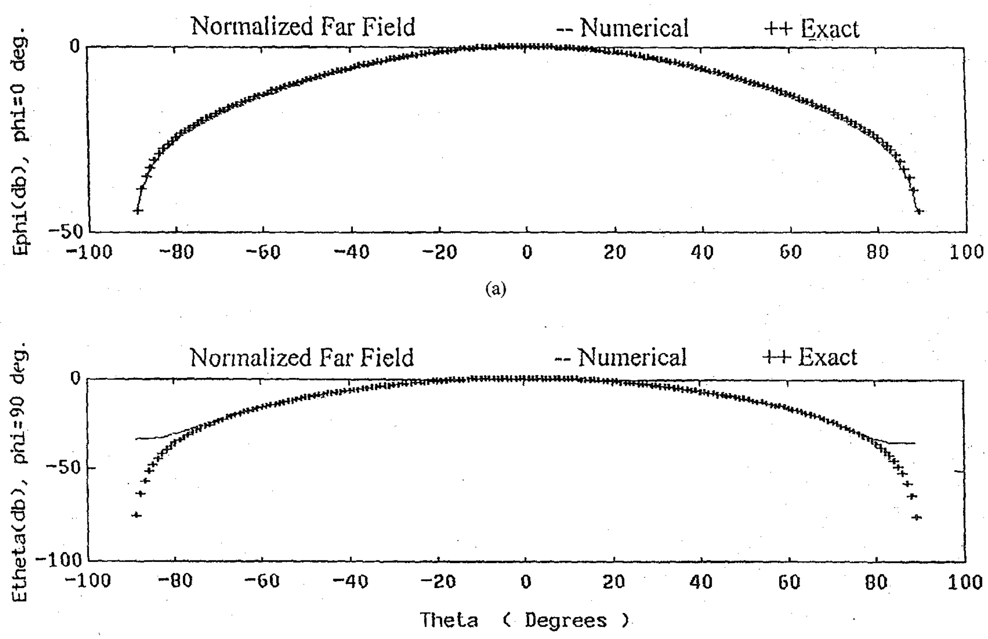

Fig. 4. (a) Comparison of exact and computed far fields ($\phi = 0°$) for sinusoidal magnetic excitation on a $1\lambda \times 1\lambda$ surface. Near field was measured on a straight line parallel to the x-axis, extending to $\pm 9\lambda$ and crossing $z = 3\lambda$. (b) Comparison of exact and computed far fields ($\phi = 90°$) for sinusoidal magnetic excitation on a $1\lambda \times 1\lambda$ surface. Near field was measured on a straight line parallel to the x-axis, extending to $\pm 9\lambda$ and crossing $z = 3\lambda$.

respectively, of the lth source point. $R_{k,l}$ is the distance between the kth field point (r_k) and the lth source point (r_l^s)

$$R_{k,l} = \sqrt{(x_k^f - x_l^s)^2 + (y_k^f - y_l^s)^2 + (z_k^f)^2}. \qquad (9)$$

The superscript f denotes the field measuring point and the superscript s denotes the source point. Note that in (8) the two subscripts i and j have been replaced by the single subscript l. That is, (x_l^s, y_l^s) is (x_i, y_j) where i and j are determined by l. Δx and Δy represent the size of the patch on S_o carrying the dipoles.

The resulting matrix (7) with (8), when solved, determines the elements of $\vec{M}_x$ and $\vec{M}_y$. This matrix equation is solved using the method of total least squares with singular value decomposition [4].

III. Numerical Results

In this section, use is made of both synthetic and experimental near field data. An attempt is made to illustrate the accuracy of the method presented here for near-field to near/far-field transformation. The results will include experiments with different antenna configurations as well as near field data taken over various geometries. As a first example, consider a four-dipole array placed at the corners of a 3.6λ by 3.6λ planar surface on the xy-plane. The center of the $3.6\lambda \times 3.6\lambda$ surface is located at $(x = 0,\ y = 0)$. At a spherical distance of 3λ from the origin with $0^\circ < \theta < 30^\circ$ and $0^\circ < \phi < 360^\circ$, on 200 discrete points, both the electric field components E_θ and E_ϕ are computed analytically. A fictitious planar surface in the xy-plane of dimensions $4\lambda \times 4\lambda$ is used to form a planar magnetic current sheet. This magnetic current sheet is divided into 10×10 magnetic current patches. The values of these currents were determined using synthetically computed near field data and choosing 114 singular values for the moment matrix. Fig. 3 compares the absolute value of the electric far-field components computed by the present method, with the exact far field computed analytically. Fig. 3(a) presents E_ϕ in db for $\phi = 0^\circ$ as a function of θ, and Fig. 3(b) presents E_θ in dB for $\phi = 90^\circ$. The comparison is visually indistinguishable. The cross polar components are negligible. Next, consider an antenna with a sinusoidal excitation. The aperture of the antenna is a square with dimension $a = 1\lambda$, whose center is placed at $(x = 0,\ y = 0)$. The excitation is x-directed and given by

$$\begin{cases} \sin\left(\frac{\pi}{2} + \frac{\pi x}{a}\right) & \text{for } \left| \begin{array}{l} -\frac{a}{2} \le x \le \frac{a}{2} \\ -\frac{a}{2} \le y \le \frac{a}{2} \end{array} \right. \\ 0, & \text{otherwise} \end{cases}$$

The near field geometry chosen for this experiment is a straight line parallel to the x-axis, extending to $\pm 9\lambda$ and crossing $z = 3\lambda$. The electric field components E_θ and E_ϕ have been computed analytically along this straight line at intervals of 0.01λ. A fictitious planar surface in the xy-plane of dimensions $1\lambda \times 1\lambda$ is used to form a planar magnetic current sheet. This magnetic current sheet is divided into 10×10 equally spaced magnetic current patches. The value of these currents were determined using synthetically computed near field data, and choosing 428 singular values for the moment matrix. Fig. 4(a) and (b) compare the absolute value of the electric far field computed by the equivalent magnetic current approach with the exact far field computed analytically. Fig. 4(a) presents E_ϕ in db for $\phi = 0^\circ$ as θ varies from -90° to 90° and, is as shown, the comparison is excellent. Fig. 4(b) presents E_θ for $\phi = 90^\circ$ as a function of θ. As observed, for θ values up to $\pm 76^\circ$, the agreement is very good. The reason for the discrepancy beyond 76° is that this cut is in a principal plane perpendicular to the plane where the near field was measured, and since we are using a straight line for the near field geometry, there is not enough information in the measured near field to correctly predict the far-field pattern for θ beyond $\pm 76^\circ$. Next, consider an antenna with a circular aperture radiating a TE_{11} mode in space. The plane of the circular aperture is on the xy-plane centered at $(x = 0.2\lambda,\ y = 0)$ with radius 0.5λ. The excitation is

$$\vec{M} = \left[\frac{x_{11}}{a} J_0\left(\frac{x_{11}}{a}\rho\right) - \frac{1}{\rho} J_1\left(\frac{x_{11}}{a}\rho\right)\right] \cos\phi\hat{\rho} - \frac{1}{\rho} J_1\left(\frac{x_{11}}{a}\rho\right) \sin\phi\hat{\phi}$$

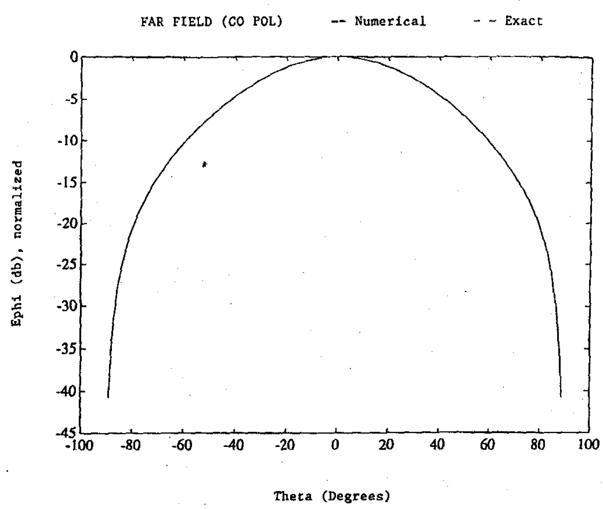

(a)

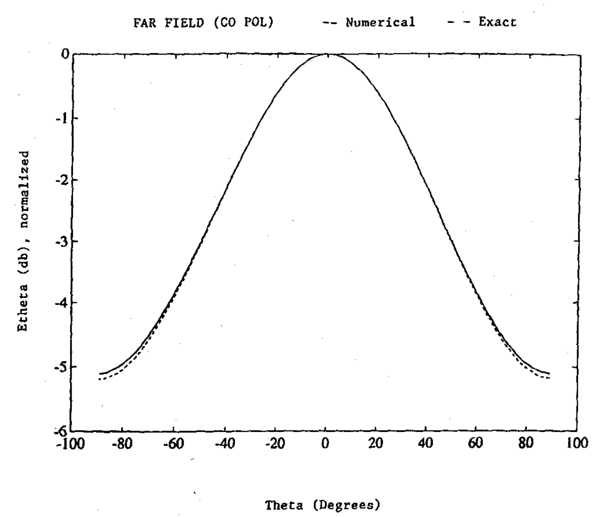

(b)

Fig. 5. (a) Comparison of exact and computed far fields (phi $= 0^\circ$) for circular aperture. (b) Comparison of exact and computed far fields (phi $= 90^\circ$) for circular aperture.

where $x = 1.841$, J_0 and J_1 are the zero and first-order Bessel functions. The near field geometry chosen for this experiment is a hemispherical surface with $r = 3\lambda$, $0 \le \theta \le 90^\circ$, and $0 \le \phi \le 360^\circ$. The simulated aperture chosen for the experiment is a rectangle with dimensions $1.5\lambda \times 1.5\lambda$ divided into 20×20 equally spaced magnetic current patches, the number of field points chosen for this experiment were 1200, and 560 singular values were chosen for the moment matrix. The copolarization patterns of the far fields obtained are depicted in Fig. 5(a) and (b). The results are compared with exact solution and, as observed, the comparison is good.

Next, experimentally measured data is utilized. Consider a microstrip array consisting of 32×32 uniformly distributed patches on a $1.5\mathrm{m} \times 1.5\mathrm{m}$ surface. The near fields are measured at discrete points on a spherical surface at a distance 1.23 m away from the antenna at a frequency of 3.3 GHz. The data is taken every 4° in ϕ for $0^\circ \le \phi \le 360^\circ$ and every 2° in θ for $0^\circ \le \theta \le 90^\circ$. Measurements have been

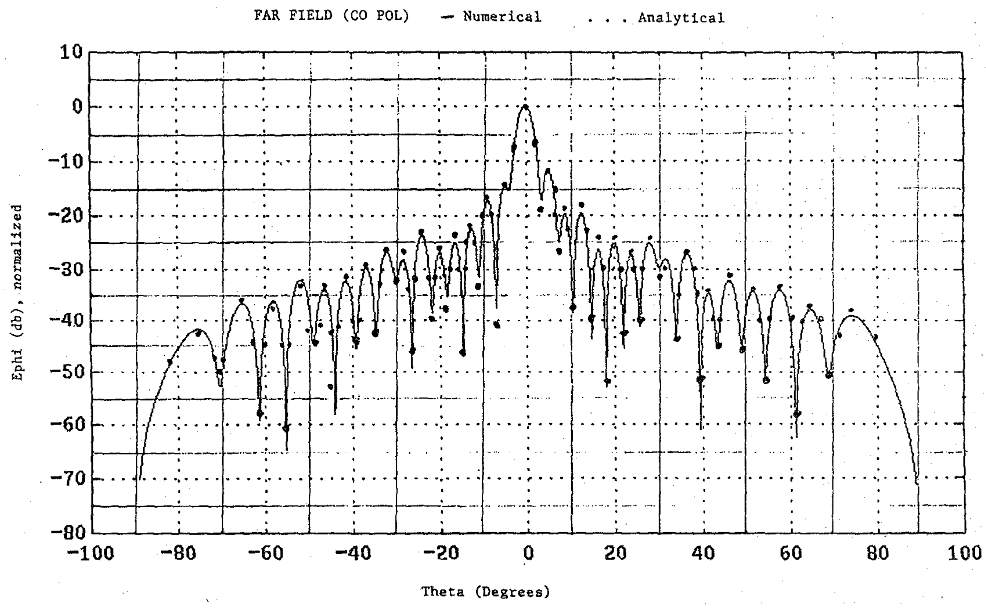

(a)

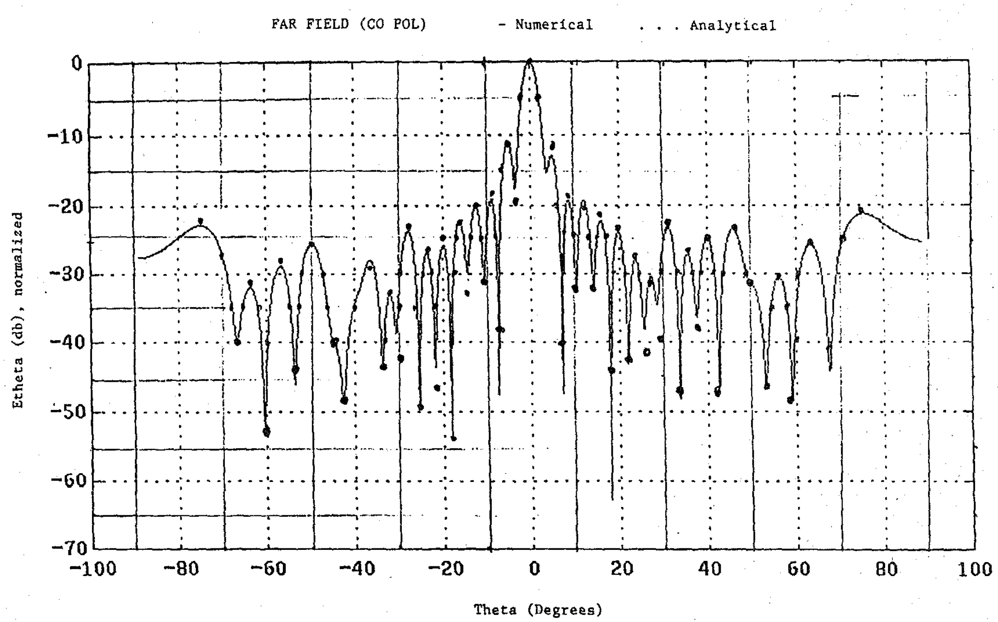

(b)

Fig. 6. (a) Copolarization characteristic for phi = 0° cut for a 32×32 patch microstrip array using numerical and analytical results. (b) Copolarization characteristic for phi = 90° cut for a 32×32 patch microstrip array using numerical and analytical results.

performed using an open ended cylindrical WR284 wave guide with the TE_{11} as the dominant mode of propagation. The measured data was provided by Dr. C. Stubenrauch of NIST. In Fig. 6, a fictitious planar surface on the xy-plane of dimensions 1.9m $\times$ 1.9m is used to form a magnetic current sheet. This magnetic current sheet is divided into 49×49 equally spaced magnetic current patches, 0.33λ apart. This figure compares the copolarization characteristic of the electric far-field pattern E_ϕ obtained by the present method with the result obtained numerically. These numerical results are the result of near-field to far-field transformation using spherical wave expansions where the fields are expanded in terms of TM and TE to r modes. Fig. 6(a) describes $20\log_{10}|E_\phi|$ for $\phi = 0^\circ$ and $-89^\circ \leq \theta \leq 89^\circ$. Near field data was measured on 8 100 discrete points located on the surface of a hemisphere at a radius of 1.23 m from the center of the antenna's aperture, and 4 230 singular values were chosen for the moment matrix. Fig. 6(b) depicts the copolarization characteristic of the electric far field for $\phi = 90^\circ$, and the same effects as before are observed. Fig. 6(c) and (d) describe the cross-polarization

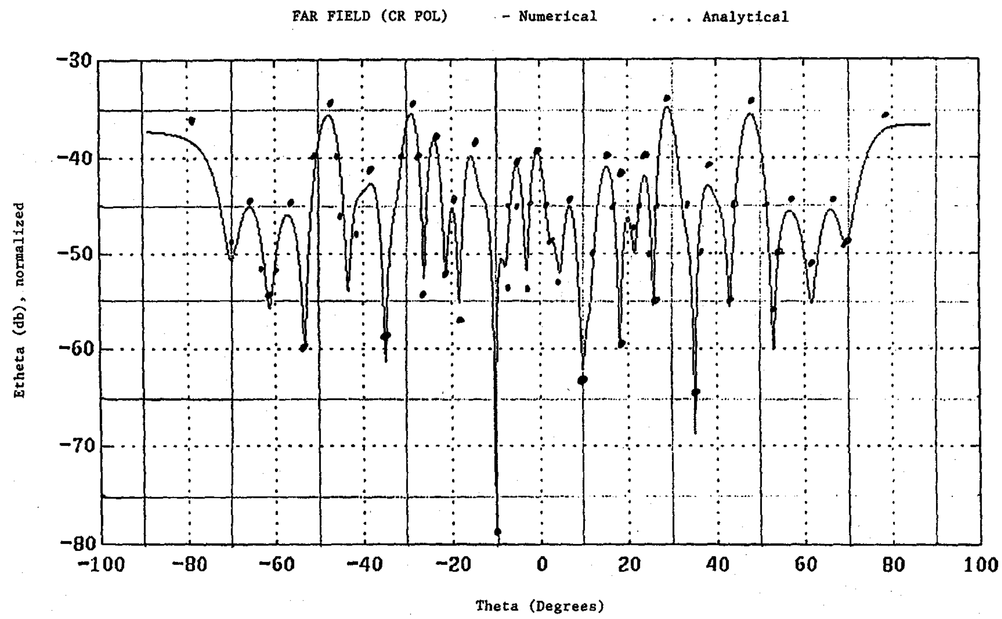

(c)

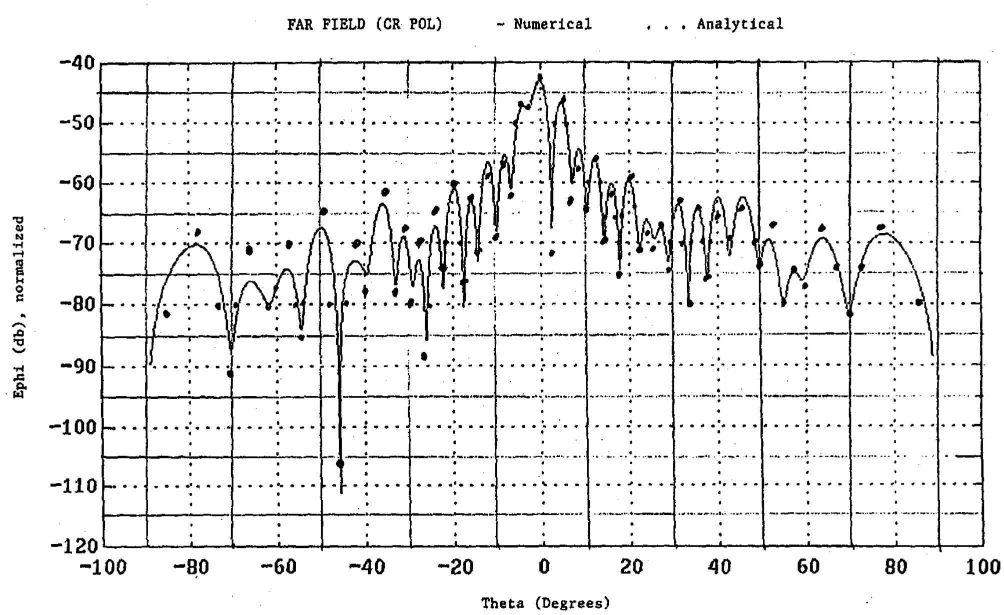

(d)

Fig. 6. *(Continued.)* (c) Cross-polarization characteristic for phi $= 0°$ cut for 32×32 patch microstrip array using numerical and analytical results. (d) Cross-polarization characteristic for phi $= 90°$ cut for 32×32 patch microstrip array using numerical and analytical results.

characteristics of the far-field patterns. Fig. 6(c) depicts $20\log_{10}|E_\phi|$ for $\phi = 90°$ and $-89° \leq \theta \leq 89°$.

IV. Conclusion

The method presented here determines the fields for $z > 0$ in front of the radiating antenna simply from the knowledge of the near field on any arbitrary geometry in space. Using various antenna configurations and near-field geometries, an investigation of the accuracy of this method was performed. For cases where synthetic sources were used, the far fields were compared with exact solutions and the agreements were quite good. For cases where actual experimental sources were used, the far fields were compared with a semi-analytical approach.

References

[1] P. Petre and T. K. Sarkar, "Planar near field to far-field transformation using an equivalent magnetic current approach," *IEEE Trans. Antennas Propagat.*, vol. 40, pp. 1348–1356, Nov. 1992.

[2] R. F. Harrington, *Field Computation by Moment Methods.* Melbourne, FL: Krieger, 1987.
[3] G. H. Golub and C. F. Van Loan, *Matrix Computations.* Baltimore, MD: Johns Hopkins University Press, 1989, 2nd ed.
[4] J. Rahman and T. K. Sarkar, "Deconvolution and total least squares in finding the impulse response of measured data from electromagnetic system," *IEEE Trans. Antennas Propagat.,* vol. 43, pp. 416–421, Apr. 1995.
[5] P. Petre and T. K. Sarkar, "Planar near-field to far-field transformation using an array of dipole probes," *IEEE Trans. Antennas Propagat.,* vol. 42, pp. 534–537, Apr. 1994.

A Novel Summation Approach in Technique to Find the Transient Response

Mohamed N. Morsy and Walter K. Kahn

***Abstract*—A novel summation variation on the usual computation by multiple reflections of the transient response for a realistically modeled pulse generator loaded with different kinds of loads is described. This constitutes an alternative method for evaluation of the inverse Laplace transform applicable for general lumped loads. As examples, we employ this approach to calculate the transient voltage response for a constant resistance and a parallel RC combination loads. The results obtained using this technique are compared with those obtained by superposition of multiple reflections.**

I. Introduction

In recent years there has emerged a definite interest in transient wave phenomena. This interest was stimulated by various applications that require the explicit treatment of pulse effects, as transmission, reception and scattering of electromagnetic fields by antennas and targets. A pulse is developed by discharging an initially charged lossless transmission line through a load, as shown in Fig. 1. The transient response for different loads has been studied extensively, [1]–[10]. In these studies, the response is obtained either as a sum of multiple reflections or as a sum of a theoretically infinite number of residue terms (singularity expansion).

The transient response, formulated as a number of successively delayed multiple reflected waves, may be computationally inconvenient for predicting the transient response at large values of time. This is because of the need to know all multiple reflections involved in producing the response for the whole preceding range of time. We present a summation approach which does not require evaluation of all of these multiple reflections. We believe this constitutes a novel variation in method for finding such transients. The basis for this approach is provided by the following readily demonstrated character of the Laplace transform. Typically, this transform of $v(t), V(s)$ appears as a sum of terms with apparent singularity at $s = 0$. Since the limit as $t \to \infty$ of $v(t) = 0$, the Laplace transform is, in fact, regular at $s = 0$. The same may be shown to hold at other apparent singular points of individual terms $s_1, s_2, \cdots$, when the transform is, in fact, an analytic function at these points. The same may be said for $i(t)$ and its transform $I(s)$.

Manuscript received December 2, 1993; revised November 6, 1995.
M. N. Morsy is with the Department of Research and Development, Armament Authority, Cairo, Egypt.
W. K. Kahn is with the School of Engineering and Applied Science, George Washington University, Washington, DC 20052 USA.
Publisher Item Identifier S 0018-9375(96)03856-2.

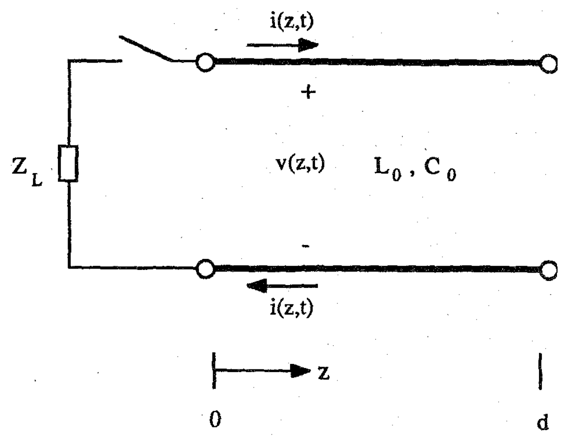

Fig. 1. Initially charged lossless transmission line.

To illustrate our technique in the simplest instance, the transient response for an initially charged lossless transmission line loaded with a resistive load is evaluated. Then our summation variation for finding the transient response is formulated for a general lumped load. Finally, this approach is carried through for a parallel $R-C, (R//C)$, circuit load. Results are compared with those obtained by conventional techniques.

II. The Transient Response for a Resistive Load

We consider the initially charged lossless transmission line, $v(z,0) = V_0, 0 < z < d$. In the system shown in Fig. 1, the line is terminated in a resistive load R. One way to get the transient response for this system is to solve the wave equation. The Laplace transform of the wave equation is

$$\frac{d^2V(z,s)}{dz^2} = L_0C_0[s^2V(z,s) - sv(z,0) - v'(z,0)]. \quad (1)$$

Given the initial values $v(z,0) = V_0, v'(z,0) = 0$ and the boundary conditions $I(d,s) = 0, V(0,s) = -RI(0,s)$, the normalized transient voltage response at the load may be expressed in the form

$$V(0,s)/V_0 = \frac{1}{s} - \frac{1}{(R+1)}\frac{1}{s[1-\rho_0\exp(-2s)]} - \frac{1}{(R+1)} \cdot \exp(-2s)\frac{1}{s[1-\rho_0\exp(-2s)]} \quad (2)$$

where $\rho_0 = (R-1)/(R+1)$ is the reflection coefficient. R is normalized to the characteristic impedance of the transmission line $Z_0 = \sqrt{L_0/C_0}$.

As previously remarked, each term of (2) has a singularity at $s = 0$. However, since (2) is an analytic function at $s = 0$, the *net* residue of the inversion integral at $s = 0$ must vanish,

$$\text{Res}[V(0,s)/V_0]\exp(st)|_{s=0} = 0. \quad (3)$$

Expanding the term $1/[1 - \rho_0\exp(-2s)]$, (2) can be written in the form

$$V(0,s)/V_0 = \frac{1}{s} - \frac{1}{s(R+1)}\Big\{1 + [\rho_0\exp(-2s)]$$